The Eurasia Proceedings of Science, Technology, Engineering & Mathematics (EPSTEM)
ISSN: 2602-3199

The Eurasia Proceedings of Science, Technology, Engineering and Mathematics (EPSTEM), 2025

Volume 38, Pages 401-414

IConTES 2025: International Conference on Technology, Engineering and Science

Impact of Printing Orientation on the Mechanical Properties of Selectively Laser Sintered PA12

Boukhoulda Farouk Benallel
Djillali Liabes University of Sidi Bel Abbes

Djellal Kouider
Djillali Liabes University of Sidi Bel Abbes

Bendine Kouider
Djillali Liabes University of Sidi Bel Abbes

Boukhoulda Abdelaziz
Djillali Liabes University of Sidi Bel Abbes

Abstract: This study explores the impact of different printing orientations in the selective laser sintering (SLS) process on the mechanical properties of polyamide 12 (PA12). Test specimens were developed according to ASTM D3039 using three distinct orientations: 0°, 45°, and 90°. Tensile tests were performed to evaluate the Young's modulus and ultimate tensile strength of each specimen tested. To complement the experimental analysis, finite element models were developed in ANSYS APDL.The models developed incorporated the Gurson-Tvergaard-Needleman (GTN) damage model, which accounts for material porosity, as well as the Chaboche model to simulate plastic deformation behavior. The numerical simulations performed closely match the experimental results, confirming the reliability of the proposed models. Microscopic observations were carried out to examine the microstructure of the printed material. The observations revealed variations in the distribution of defects and porosity and demonstrated that this originates from the printing orientation of the material. For certain orientations, the specimens showed more uniform microstructures and fewer defects, which correlates with better mechanical properties, such as increased stiffness and strength. These results highlight the very important role of printing orientation in optimizing the structural integrity and mechanical performance of PA12 components manufactured by SLS, while validating the predictive capacity of the numerical approach.

Keywords: PA12, 3d printing, SLS, Tensile, Modeling

Introduction

Additive Manufacturing (AM) has emerged as a rapidly growing technology in modern industry, providing the ability to fabricate complex geometries and customized components with high efficiency. Among the various AM processes, Selective Laser Sintering (SLS) is one of the most widely used for polymer-based applications due to its good dimensional accuracy and favorable mechanical performance. Polyamide 12 (PA12) is commonly employed as a reference material in SLS, valued for its balanced combination of mechanical strength, chemical resistance, and processability. However, a major challenge in SLS fabrication lies in the occurrence of porosity, which can significantly influence the strength, durability, and overall performance of printed parts.

SLS employs one or more lasers to selectively fuse polymer particles layer by layer within a controlled environment. This process is highly intricate and demands rigorous control to ensure successful printing and high-quality parts (Bendine et al., 2022; Bourell, 2016; Charoo et al., 2020; Rajesh et al., 2015; Senthilkumaran et al.,

- Selection and peer-review under responsibility of the Organizing Committee of the Conference

2009; Simha Martynková et al., 2021; Stoia et al., 2019)**.** A significant advantage of SLS is its ability to minimize raw material waste while enabling the production of complex geometric shapes with minimal limitations, unlike traditional manufacturing methods. Among the materials used in SLS, polyamide 12 (PA12) stands out due to its ease of use, efficiency, and a broad temperature window between the onset of melting during heating and crystallization during cooling. This wide thermal range allows PA12 to remain heated without crystallizing until the cooling stage, enhancing part consolidation and preventing warping (Dadbakhsh et al., 2017; Mwania et al., 2020)**.** Additionally, PA12 boasts excellent mechanical properties, low moisture absorption compared to other polyamides, and strong resistance to abrasion and chemicals, including solvents (Dadbakhsh et al., 2017). The mechanical properties of SLS-fabricated parts are influenced by both the raw material characteristics and process parameters. Numerous studies have demonstrated that factors such as powder bed temperature, powder composition, the use of additives, printing speed, printing orientation, and varying laser energy densities significantly affect the final material properties (Amado-Becker et al., 2008; de Oliveira Setti et al., 2014; Hopkinson et al., 2009)**.**

More particularly, the printing orientations, which can be done in several directions, have a significant influence on the mechanical properties (Rodríguez et al., 2023). Indeed, several researchers (Caulfield et al., 2007; Olejarczyk et al., 2020; Stichel et al., 2017; Tomanik et al., 2021) have undertaken tensile tests to show this influence. The results agree that the printing strategy is crucial for the resistance of specimens subjected to axial load. Some researchers like Ajoku et al. (Ajoku et al., 2006) showed that the most optimal mechanical properties (tensile strength, Young's modulus, elongation at break) were observed for specimens printed in the plane of the powder bed (an angle of 0°) and showed that a difference of 16% in terms of resistance and 11.2% in modulus observed between the two orientations (0° and 90°). In another work, (Caulfield et al., 2007) found that parts oriented at 0° have a higher breaking strength value than 90° and parts oriented at 90° have higher breaking elongation values to those of 0° oriented parts. This observation was also made by Tomanik et al. (Tomanik et al., 2021)**.** They concluded that the specimens printed at 0° presented a more ductile behavior than those printed at 45° and also showed that the best mechanical properties are obtained for parts printed with an angle of 0°, i.e. that is to say in the plane of the powder bed. El Magri et al. (El Magri et al., 2022)studied the influence of the printing angle on the tensile strength (TS). They found that the 90° plane orientation exhibits (TS) values 2 to 10% lower than those of 0°, with the largest difference observed at low laser power. Usher J.S. et al. (Usher et al., 2013)**.** They found that specimens built in the 90° orientation exhibit much lower elongation values (around 12–13%) than those built in the 0° orientation. It was also observed that specimens constructed in the 90° orientation required a much higher energy density to achieve a stable elongation value.

Results from previous literature searches suggest that the printing angle significantly influences the mechanical properties of SLS specimens, and an optimal orientation can be chosen based on the specific strength and stiffness requirements of the components. They have also shown through tensile tests, and sometimes through tomographic analyzes (Dupin et al., 2012; Rosso et al., 2020; Stichel et al., 2017) the existence of an anisotropy of the material (Cano et al., 2018). For example, (Obst et al., 2018; Sindinger et al., 2020) confirmed that residual voids aligned perpendicular to the loading direction are the main factor that explains structural anisotropy. According to research, porosity can occur due to several parameters: inconsistency of powder deposition and incomplete fusion of particles (Bourell et al., 2014; Dupin et al., 2012; Majewski et al., 2008; Stichel et al., 2017; Toth-Taşcău et al., 2012; Zárybnická et al., 2022), type of conditioning and drying of PA12 powder, low viscosity, coalescence, atmospheric gas trapped between particles and layers and off-gassing of degradation products. Bain et al. (Bain et al., 2019) confirms that the porosities present between the layers cause weak interfaces and thus affect the overall strength of the part. Porosity must therefore be imperatively controlled by choosing the appropriate manufacturing process to guarantee product quality. It is also necessary to control the process parameters such as: temperature, layer thickness, scanning spacing, energy density provided by the laser and orientation of the construction. Calignano et al. (Calignano et al., 2021) depending on the orientation of the specimen and the printing technology, the porosity levels and pores have different morphology and distribution in the sample. A close correlation was highlighted between the pores and their descriptors and the mechanical behaviour of the specimen. There are mathematical models in the literature that take into consideration the presence of porosities to describe the behavior of materials (Roszak et al., 2021; Schob et al., 2019).

In this study, the effect of printing direction on the mechanical properties, specifically Young’s modulus and ultimate tensile strength, was thoroughly investigated. To achieve this, tensile tests were conducted on specimens printed at different orientations, adhering to standardized procedures in compliance with ASTM D3039. As an innovative approach, a detailed microscopic analysis of the printed parts was performed using scanning electron microscopy (SEM) to examine and analyze the microstructural characteristics. This dual investigation-combining mechanical testing with microscopic analysis-not only provided valuable insights into the influence of printing

direction on the mechanical behavior of the material but also highlighted the critical role of microstructural features such as porosity and layer bonding in determining overall performance.

Materials and Methods

Experimental Procedure and Devices

Materials

The material employed in this study was Polyamide 12 (PA12), a thermoplastic polymer widely used in additive manufacturing owing to its outstanding mechanical performance, chemical resistance, and thermal stability. PA12 is particularly advantageous for Selective Laser Sintering (SLS) processes because of its relatively low melting temperature, uniform particle morphology, and excellent flowability. The powder utilized exhibited a particle size distribution between 20 µm and 40 µm, which falls within the typical range for high-resolution SLS applications (see Figure 1).

Figure 1. Polyamide 12 (Nylon PA12) powder

SLS Printing Machine Used

The 3D printer used is the MfgPro230 xS from Formlabs. This printer is designed for professionals in the aerospace and automotive sectors, as well as those who need to create advanced prototypes. It offers a build volume of 230 x 230 x 230 mm. The layer thickness is 0.1 mm. It is compatible with materials such as nylon, PC (polycarbonate), and other similar thermoplastics. The machine is compatible with SLS Build and SLS Ware software. It is ideal for industries looking to develop end-use parts with high mechanical performance (see figure 2).

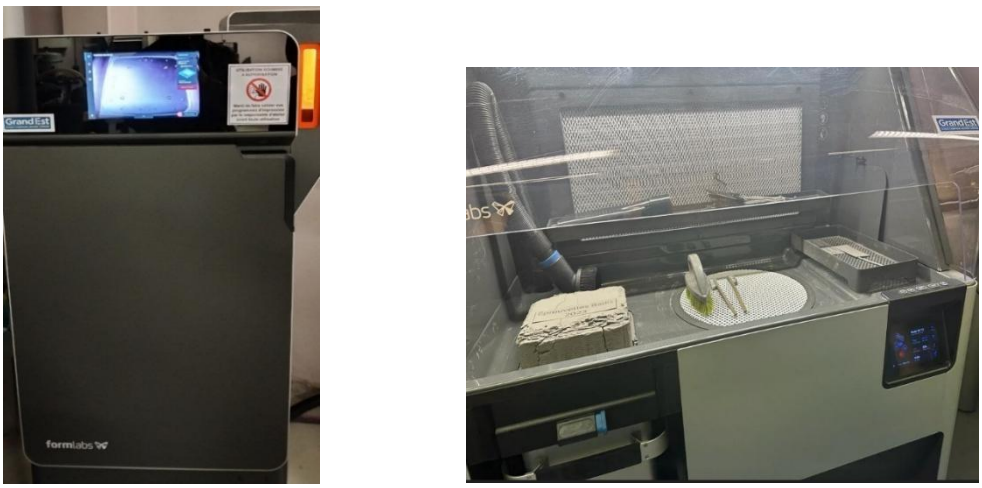

Figure 2. The SLS machine (Formlabs MfgPro230 xS printer)

The printer's operating principle is shown in Figure 3 below: The selective laser sintering (SLS) process is based on the layer-by-layer selective fusion of polymer powder using a laser beam. Initially, a thin layer of powder is deposited and evenly spread over the build platform by means of a steel recoating roller, which may also be heated to ensure uniform powder distribution. The build chamber is typically maintained under an inert gas atmosphere (such as nitrogen or argon) to prevent powder oxidation. To facilitate sintering and reduce the required laser power, the powder bed is preheated by infrared (IR) radiation to a temperature close to the polymer's melting point. The build platform then lowers by a distance equal to the desired layer thickness, while the powder supply platform rises by the same amount to allow the deposition of a new powder layer. The laser parameters and scanning paths are predefined based on the digital model generated through computer-aided design (CAD). The laser beam selectively heats the powder according to the geometry of each cross-sectional layer of the model, raising the temperature of the particles to a point where solid-state diffusion and coalescence occur between adjacent grains. The surrounding unsintered powder acts as a natural support for subsequent layers. This sequence of deposition, selective sintering, and platform adjustment is repeated layer by layer until the complete three-dimensional part is fabricated. Various parameters must be correctly set, including laser power, powder scanning diameter and speed, scan spacing, preheating, etc.

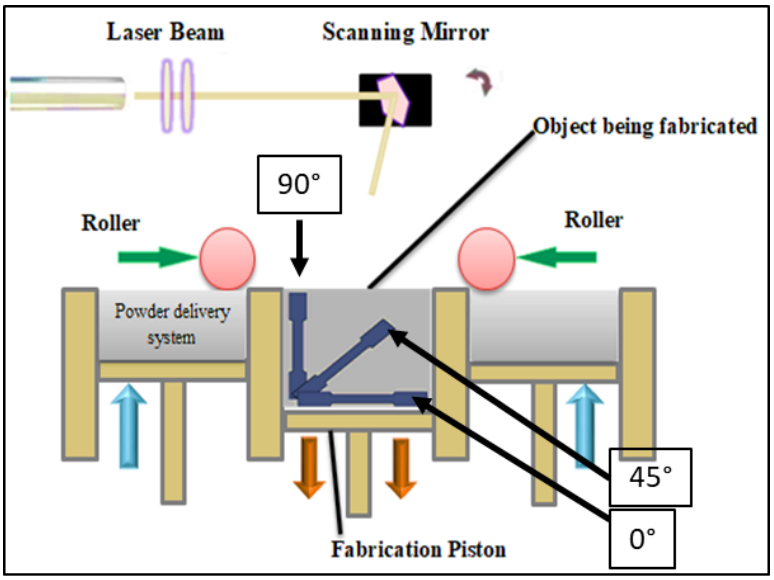

Figure 3. Illustration of printing angles

Tensile Machine

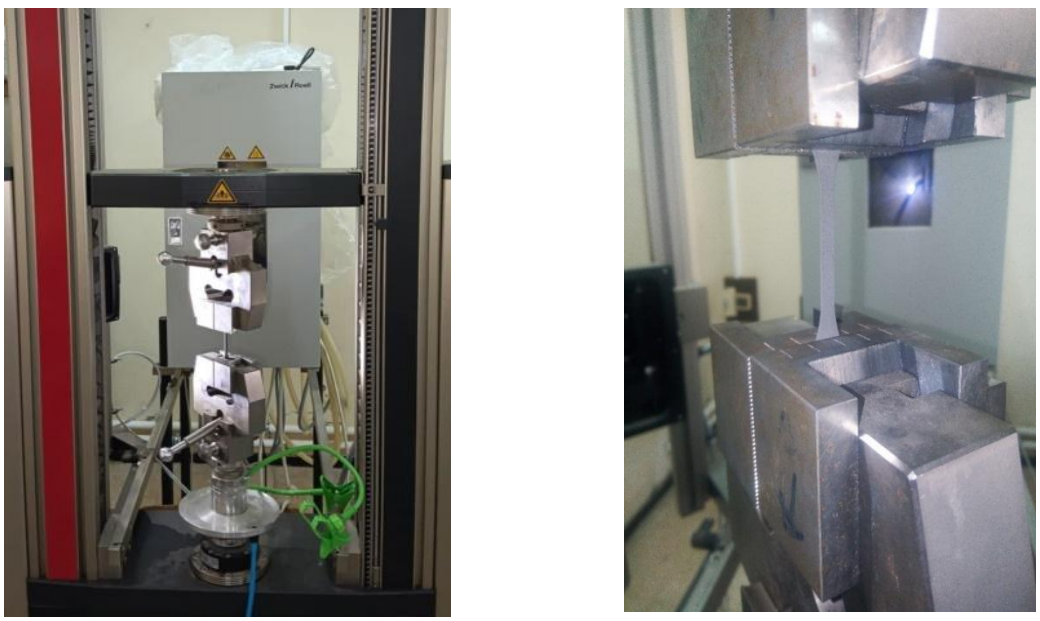

Figure 4. Tensile machine (Zwick, 25KN)

Tensile testing was conducted using a Zwick 25KN testing machine (Figure 4). The specimens were loaded until failure, and data on load vs. displacement were recorded for analysis. The machine is used for tensile and compressive testing. It features a high-rigidity frame and a highly accurate beam steering mechanism, ensuring positioning accuracy of approximately ±2 µm, thanks to the use of a Hiperface® recipr;:: :ocating servomotor and the testControl II electronic system. The tabletop model typically has a height of approximately 1050 mm and a width of approximately 440 mm, providing ample space for sample and equipment setup. This configuration allows for obtaining an accurate stress-strain curve for an SLS polyamide 12 sample, particularly regarding deformation due to gripper slippage or velocity fluctuations, and ensuring consistent collection of load and strain data throughout the test interval.

Specimens of Tensile Test

To characterize the printed material, standardized tensile test specimens were fabricated by selective laser sintering (SLS) from PA12 powder. Three printing angles were considered: 0°, 45°, and 90°, as illustrated in Figure 5. In this study, nine polyamide 12 (PA12) specimen were manufactured. The specimen were printed in three different orientations: 3 specimen at 0°, 3 specimen at 45° and 3 specimen at 90°. To ensure the correct orientation of each sample after printing and to avoid confusion during mechanical testing, a simple physical coding system was adopted: Specimen printed at 0° have no chamfer (no markings). Specimen printed at 45° have one chamfer at their end. Specimen printed at 90° have two chamfers at their end. This system allowed for quick visual differentiation between groups of samples after printing and during tensile testing (see Figure 4(b).

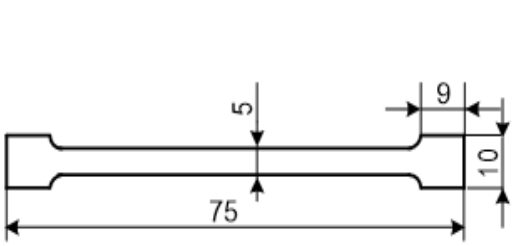

(a): Geometry of the ASTM test specimen (Thickness = 2mm).

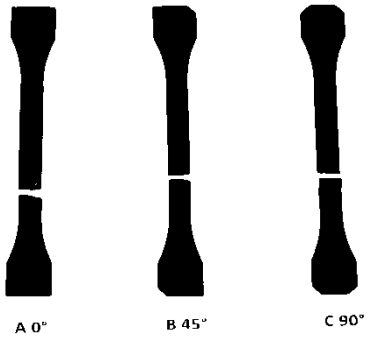

(b): PA12 specimen broken by traction

Figure 5. PA12 specimen of traction

Identification of Two Behavior Models

Gurson-Tvergaard-Needleman Damage Model

In the proposed numerical approach, the model integrates the Gurson-Needleman and Tvergaard (GTN) behaviors to account for the presence of voids within the 3D printed specimens. This combination of models allows for a more comprehensive understanding of material response, taking account the complex interactions associated with void formation and growth. GTN is a combination between Gurson model and Needleman and Tvergaard that considers damage in the material, which is mainly used, in ductile model. The model assumes that the plasticity and damage in the material are mainly driven by the voids three state which are void growth, nucleation and coalescence on a microscopic level. GTN model reflects the three states of voids as a changing of void volume fraction and the resulting pressure. Thus, GTN formulates the yield criteria as follow:

$$F = \frac{\sigma_{eq}^2}{\sigma_y^2} + 2f^* q_1 \cosh\left(\frac{3}{2} q_2 \frac{\sigma_m}{\sigma_y}\right) - (1 + q_3 (f^*)^2) \geq 0 \qquad (1)$$

Where q_1, q_2 and q_3 are fitting parameters,
σ_y, σ_{eq} Are the yield strength and the Von Mises equivent stress respectively,
σ_m is the hydrostatic stress defined as the average of the normal stress components,
f^* is the modified void volume fraction used to model the loss of load carrying capacity due to void coalescence and it is given by equation bellow,

$$f^* = \begin{cases} f_0 & if \quad t = 0 \\ f & if \quad f \leq f_c \\ f_c + \frac{f_f^* - f_c}{f_f - f_c}(f - f_c) & if \quad f_c < f \leq f_f \end{cases} \tag{2}$$

The initial porosity f_0 is determined at time $t = 0$ and serves as the starting point for the void volume fraction evolution. Throughout the deformation process. The total void volume fraction f evolves over time due to both according to:

$$f = 1 - \frac{V_M}{V} \tag{3}$$

Where V and V_M are the volume of the material with and without defects respectively,
f_c is the critical volume fraction of the pores at which the voids start to unite and f_f^* gives the ultimate value of f^* at which the stress carrying capacity goes to zero,
f_f is the void volume fraction corresponding to fracture.
The rate of void volume fraction depends on both void growth and void nucleation, ie

$$\dot{f} = \dot{f}_{gr} + \dot{f}_{nucl} \tag{4}$$

Where the rate of void growth, f_{gr}, is given by the following relation

$$f_{gr} = (1 - f)\dot{\epsilon}_{kk}^{pl} \tag{5}$$

Where $\dot{\epsilon}_{kk}^{pl}$ is the plastic hydrostatic strain.
The rate of void nucleation is given by the equation (6)

$$\dot{f}_{nucl} = \frac{f_N}{S_N\sqrt{2\pi}} exp\left[-\frac{1}{2}\left(\frac{\epsilon^{pl} - \epsilon_N}{S_N}\right)^2\right]\dot{\epsilon}^{pl} \tag{6}$$

Where f_N is the nucleation micro-void volume fraction,
Furthermore, S_N is the standard deviation and ϵ_N is the mean in the Gaussian distribution that is assumed for the void nucleation rate.

Chaboche Model

According to the literature such as (Schob et al., 2023), it was observed that the PA12 material manufactured by the SLS process exhibited viscoplastic behavior (Schob et al., 2023). The behavior was described by the Chaboche model which is made up of a system of differential equations. Taking into account small deformations, this model results from the additive decomposition of the total strain rate $\dot{\varepsilon}^{tot}$ into an elastic part denoted $\dot{\varepsilon}^{el}$ and viscoplastic part noted $\dot{\varepsilon}^{vp}$.

$$\dot{\varepsilon}^{tot} = \dot{\varepsilon}^{el} + \dot{\varepsilon}^{vp} \tag{7}$$

$$\dot{\sigma} = \mathrm{E}(\dot{\varepsilon}^{tot} - \dot{\varepsilon}^{vp}) \tag{8}$$

Where $\boldsymbol{\sigma}$ is stress and **E** Young modulus.

The Chaboche model described here contains three parameters in its original form which are determined experimentally. These are the Young modulus E and the two hardening parameters γ_i and C_i. Depending on how many counter-constraints are used, the number of parameters changes.

$$\dot{\varepsilon}^{vp} = \dot{\lambda}.n = \dot{\lambda}\left\{\frac{\partial\varphi}{\partial\sigma}\right\} = \sqrt{\frac{2}{3}\varepsilon^{vp}:\varepsilon^{vp}}\,\frac{3}{2}\frac{s - \sum_{i=1}^{n}\alpha_i}{\sigma_y} \tag{9}$$

$$\dot{\alpha}_i = \frac{2}{3}C_i\dot{\varepsilon}^{vp} - \gamma_i\alpha_i\dot{p} \tag{10}$$

The definition of the viscoplastic strain rate is decisive. These are the viscoplastic multiplier $\dot{\lambda}$ and the direction n. The flow function φ is the closure of the elastic domain. The flow function depends on the one hand on the elastic limit σ_y, on the deviatoric stress value s and on the other hand, on the kinematic hardening. The kinematic hardening is taken into account by the counter-constraints $\dot{\alpha}_i$. This is described by the accumulated plastic strain $\dot{p}$and the hardening parameters C and γ.

Finite Element Model

The finite element models proposed in the present analysis were designed, implemented and carried out using ANSYS APDL. In the initial phase, key points were strategically positioned during the design stage to define the model's geometry. Subsequently, lines and areas were created, forming the basis for extracting a three-dimensional volume. The mesh generation process employed solid185 elements, each featuring 8 nodes with three degrees of freedom. The model underwent meticulous boundary condition application in alignment with the experimental procedure. Material properties were judiciously assigned to the model, and for heightened accuracy, both GTN and Chaboche models were integrated to address factors such as porosity and the plasticity zone. This holistic approach ensured the creation of a robust and representative finite element model for subsequent analyses. Notably, the model accounted for the impact of printing orientation by introducing degradation in Young's modulus and tensile strength, inspired by the outcomes of the experimental tests. A sensitivity analysis guided the selection of 6080 elements, deemed suitable for all simulations. In terms of analysis, a quasi-static approach using the Newton-Raphson method scheme was employed, employing an imposed displacement for stability, executed over 100 steps. The numerical model is depicted in Figure 6 bellow. The full implemented code for the purpose is given in the appendix. To accurately simulate he porosity of the blank sample, the initial porosity f_0 as measured at $t = 0$. Due to variations in the initial porosity values obtained from different analyses, an average value of 3.57% was selected. In addition to the initial porosity, damage parameters $q_1, q_2, f_N, \varepsilon$ and $S_N$were established using a specialized adjustment tool. These refined settings were subsequently implemented in ANSYS 17.2 to enhance the model's accuracy.

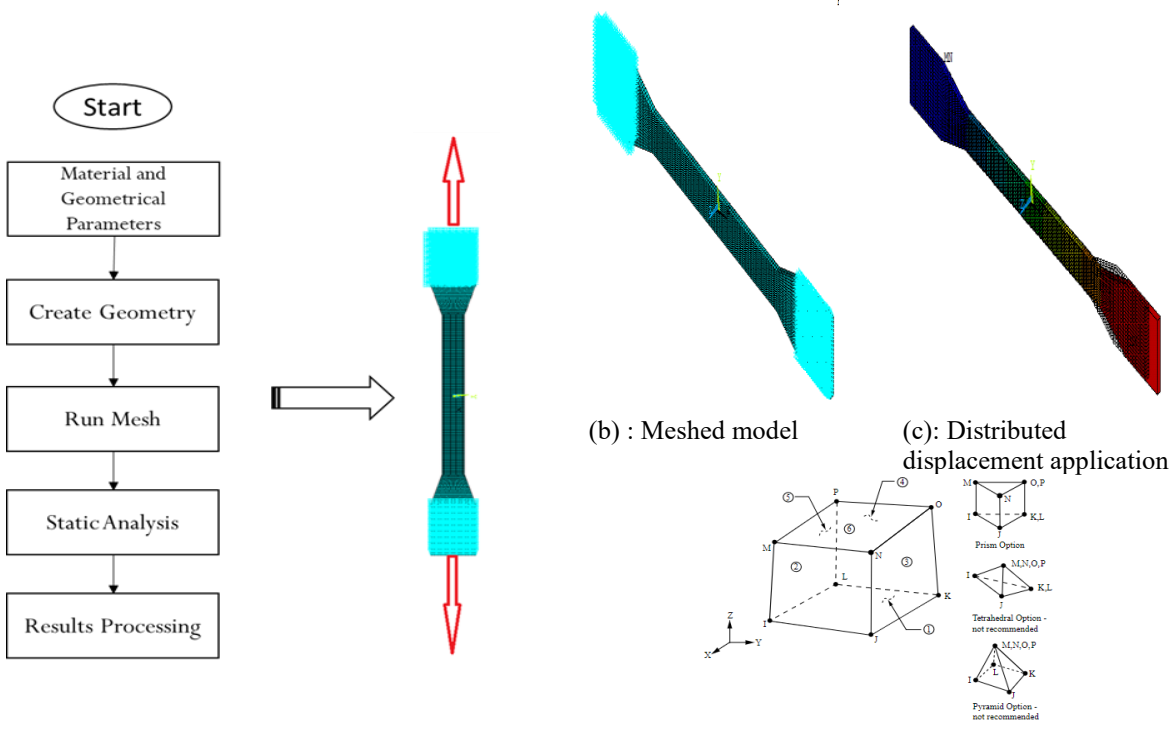

(a) : Numerical procedure flowchart (b) : Meshed model (c): Distributed displacement application (d) : Solid185 element in Ansys

Figure 6. Finite element model

Results and Discussion

This section presents and analyzes the results obtained. The analysis focuses on tensile tests and associated numerical models, followed by a detailed analysis of the microstructural properties of the printed parts.

Tensile Tests

Experimental Results

A total of three tensile tests were conducted for each printing angle, and the results are illustrated in Figure 7. The observed differences in Young's modulus and tensile strength among specimens printed at different angles suggest a correlation between printing orientation and mechanical properties. The observed variations in Young's modulus and tensile strength across different printing angles are further elucidated through Figures 8 and 9. The results shown that the specimens printed at 0°are displayed, the superior Young's modulus and tensile strength indicate that this specific printing orientation contributes to enhanced mechanical performance. This result aligns with the notion that printing in-plane corresponding to 0° may lead to a more structurally sound and less porous arrangement of material. The printing process, when perpendicular to the laser projection, likely results in a more densely packed structure, reducing porosity and improving material integrity.

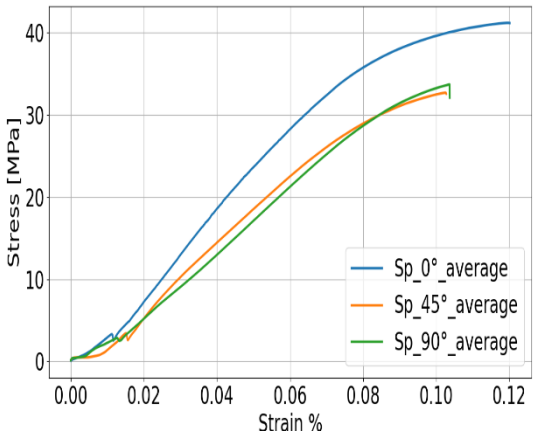

Figure 7. Stress–strain curves for specimens tested at 0°, 45°, and 90° orientations

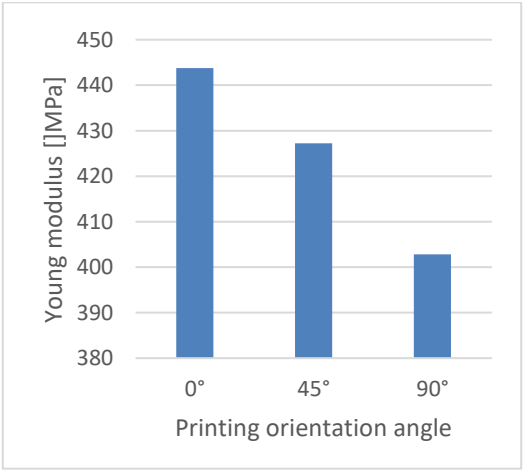

Figure 8. Young's modulus as function as printing orientation angle

Figures 9 and 10 shows respectively the variation of the ultimate strength and the elongation at break as function as the printing orientation angle.

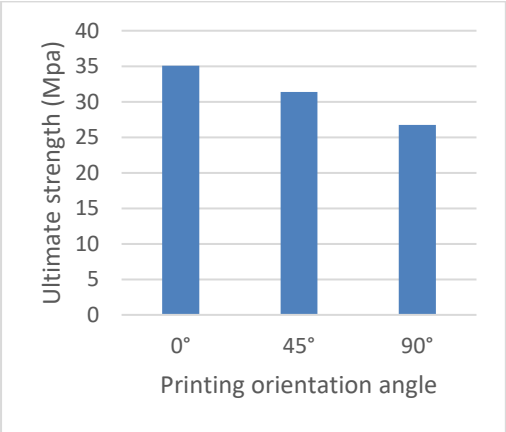

Figure 9. Ultimate strength UTS

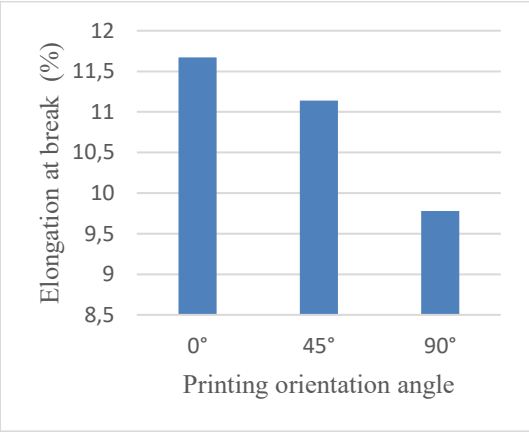

Figure 10. Elongation at break

Table 1. Tensile properties of SLS PA12 polyamide

Orientation Angle [°]	Elastic modulus (MPa)	Ultimate strength UTS (MPa)	Elongation at break (%)
0	443,79±6,92	35,09±1,82	11,67±0,33
45	427,24±2,89	31,39±1,72	11,14±0.9
90	402,85±3,91	26,72±1,65	9,78±0,77

Specimens printed at 45° and 90° angles exhibit lower Young's modulus values compared to those printed at 0°.

Numerical Results

The results of the modeling used in the Ansys software are shown in Figures 11-13 below, corresponding to the tests on the printed specimens at 0°, 45° and 90° respectively.

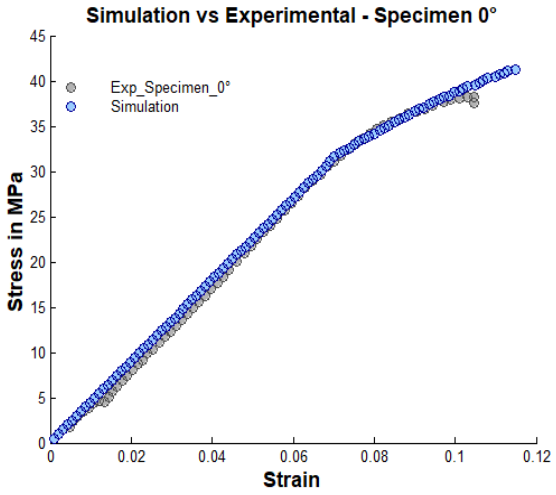

Figure 11. Modeling the tensile behavior of the specimen printed at 0°

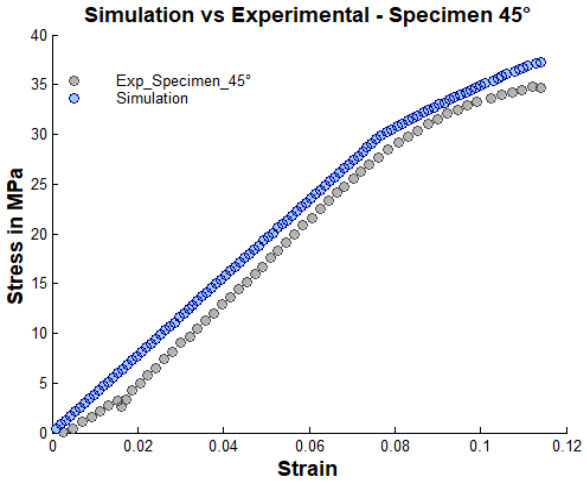

Figure 12. Modeling the tensile behavior of the specimen printed at 45°

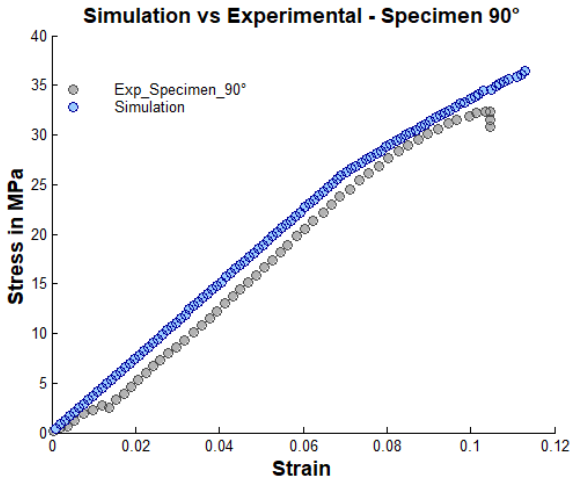

Figure 13. Modeling the tensile behavior of the specimen printed at 90°

Porosity Analysis

To evaluate the porosity, a combination of advanced imaging and digital image processing techniques was utilized. High-resolution optical microscopy was employed to acquire cross-sectional images of the specimens fabricated at different build orientations (see Figure 14). All images were captured under identical lighting and magnification conditions to ensure consistency and reliable comparison.

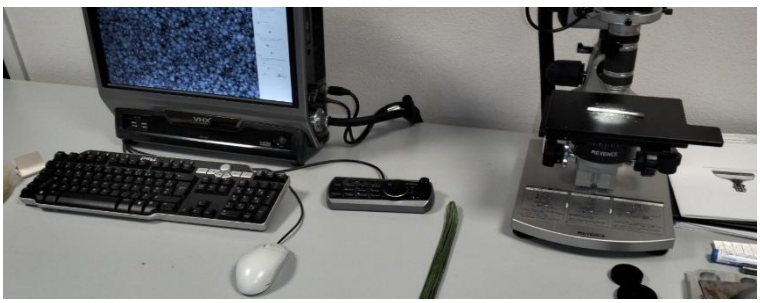

Figure 14. High-resolution optical microscopy

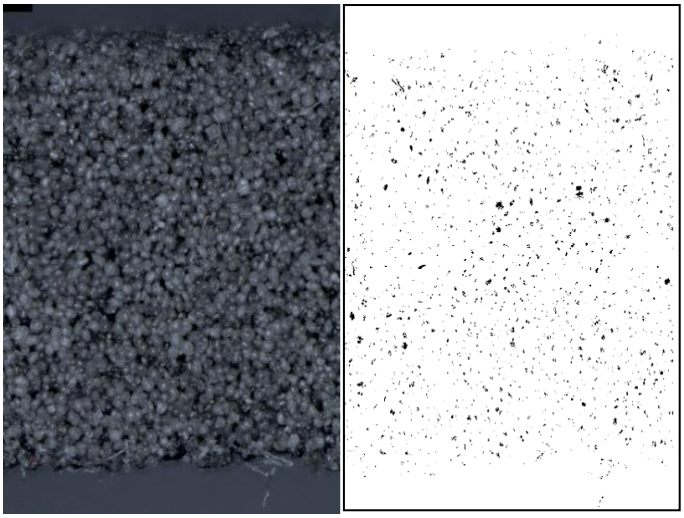

Figure 15. Observation on the 0° test specimen (Porosity rate between 4.80% and 5.93%)

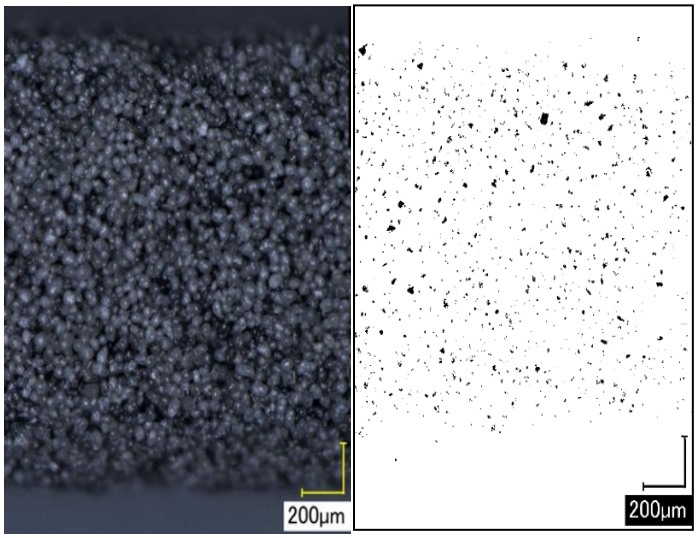

Figure 16. Observation on the 45° test specimen (Porosity rate between 5.12% and 6.40%)

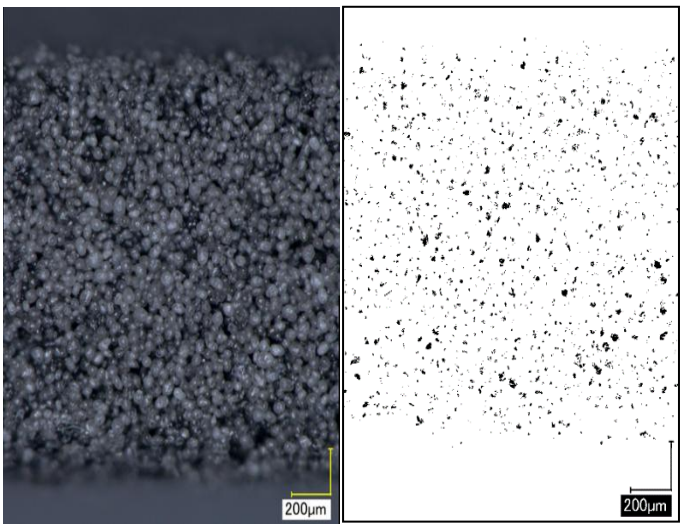

Figure 17. Observation on the 90° test specimen (Porosity rate between 7.10% and 8.32%)

Porosity quantification was performed through a custom-developed Python script incorporating the OpenCV and NumPy libraries. The image processing workflow included the following steps:

1. Grayscale conversion: Each image was converted to grayscale to enhance the contrast between the polymer matrix and the voids, thereby facilitating more accurate segmentation.
2. Thresholding: A global thresholding approach was applied to differentiate the solid regions from the pores. The Otsu algorithm was used to automatically determine the optimal threshold value.
3. Segmentation and morphological filtering: Following thresholding, morphological operations such as erosion and dilation were employed to reduce image noise and refine pore boundaries.
4. Porosity calculation: The porosity was determined as the ratio of the total pore area to the overall image area, expressed as a percentage according to the relation:

$$\text{Porosity} = \frac{\text{Void Area}}{\text{Total Area}}$$

The surface porosity analysis revealed a clear influence of build orientation on the porosity rate of SLS-fabricated PA12 specimens. Samples printed at 0° exhibited the lowest porosity, ranging from 4.8% to 5.93%, indicating a relatively dense structure with minimal void formation. At 45°, the porosity slightly increased to values between 5.12% and 6.4%, suggesting that the intermediate orientation leads to less efficient particle fusion compared to the horizontal build. The highest porosity was observed at 90°, with values ranging from 7.1% to 8.32%, which can be attributed to reduced interlayer bonding and weaker laser energy distribution along the vertical direction. Based on the obtained results (Figures 15, 16 and 17), a histogram was plotted to illustrate the variation of the porosity rate as a function of the printing angle (see Figure 18). This representation provides a clear visualization of how build orientation influences the formation and distribution of pores within the printed specimens.

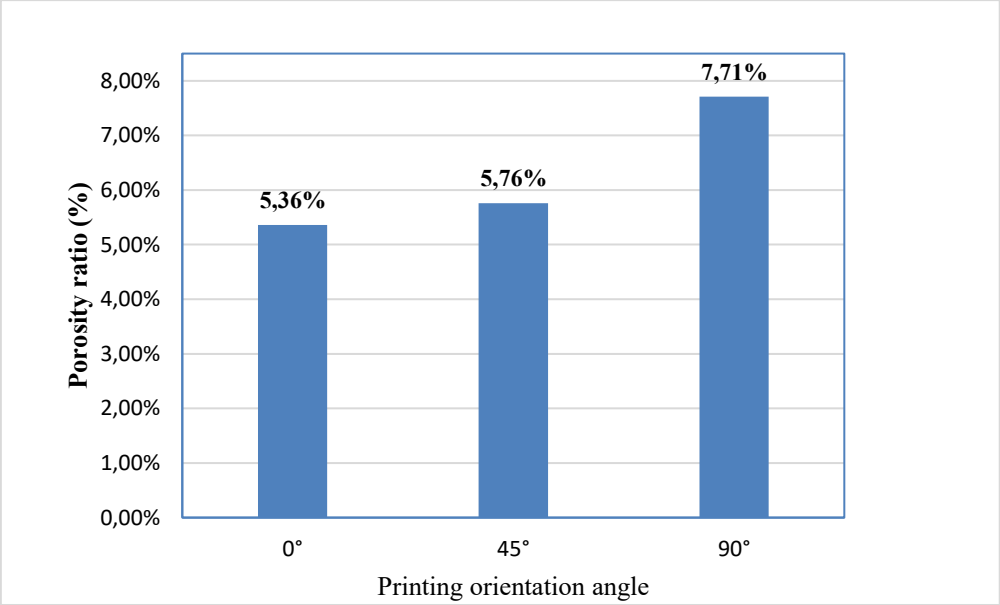

Figure 18. Effect of build orientation on the surface porosity before tensile testing

As suggested by (Cano et al., 2018), printing orientations other than 0° introduce geometric and thermal challenges that further exacerbate the formation of voids and defects. This underscores the critical importance of optimizing printing parameters to achieve improved mechanical properties in additively manufactured components.

Conclusion

This study investigated the effect of printing angle on the mechanical properties of 3D printed PA12 through tensile testing in accordance with ASTM D3039. The main conclusions are as follows:

- Variations in mechanical properties based on printing angles highlight the importance of considering the orientation of printed parts during the additive manufacturing process. The findings suggest that adjusting the printing angle can be a critical factor in optimizing the mechanical performance of PA12 components.
- Tensile test results showed that samples printed at 0 degrees have higher Young's modulus and tensile strength than other orientations. This specific printing orientation contributes to improved mechanical

performance of the material, aligning with the idea that printing in the 0° plane can lead to a structurally stronger and less porous arrangement.
- The observed decrease in mechanical properties is attributed to anisotropic behavior and the presence of porosities at non-zero printing angles.
- These findings emphasize the need for precise control of the printing direction to obtain good mechanical properties and a uniform distribution of porosity.

Scientific Ethics Declaration

* The authors declare that the scientific ethical and legal responsibility of this article published in EPSTEM journal belongs to the authors.

Conflict of Interest

* The authors declare that they have no conflicts of interest

Funding

* This study was funded by the Science Committee of the Ministry of Science and Higher Education of the Republic of Kazakhstan (Grant No. AP19678682).

Acknowledgements or Notes

* This article was presented as a poster presentation at the International Conference on Technology, Engineering and Science (www.icontes.net) held in Antalya/Türkiye on November 12-15, 2025.

* The authors thanks Prof. Nouari Mohammed and Dr. Badis Haddag, research professors at the University of Lorraine, France, for their unwavering support, valuable guidance, and continuous encouragement throughout this work.

References

Ajoku, U., Saleh, N., Hopkinson, N., Hague, R., & Erasenthiran, P. (2006). Investigating mechanical anisotropy and end-of-vector effect in laser-sintered nylon parts. *Proceedings of the Institution of Mechanical Engineers, Part B: Journal of Engineering Manufacture*, *220*(7), 1077-1086.

Amado-Becker, A., Ramos-Grez, J., José Yañez, M., Vargas, Y., & Gaete, L. (2008). Elastic tensor stiffness coefficients for SLS Nylon 12 under different degrees of densification as measured by ultrasonic technique. *Rapid Prototyping Journal*, *14*(5), 260-270.

Bain, E. D., Garboczi, E. J., Seppala, J. E., Parker, T. C., & Migler, K. B. (2019). AMB2018-04 : Benchmark Physical Property Measurements for Powder Bed Fusion Additive Manufacturing of Polyamide 12. *Integrating Materials and Manufacturing Innovation*, *8*(3), 335-361.

Bendine, K., Gibhardt, D., Fiedler, B., & Backs, A. (2022). Experimental characterization and mechanical behavior of 3D printed CFRP. *European Journal of Mechanics-A/Solids*, *94*, 104587.

Bourell, D. L. (2016). Sintering in laser sintering. *JOM*, *68*(3), 885-889.

Bourell, D. L., Watt, T. J., Leigh, D. K., & Fulcher, B. (2014). Performance limitations in polymer laser sintering. *Physics Procedia*, *56*, 147-156.

Calignano, F., Giuffrida, F., & Galati, M. (2021). Effect of the build orientation on the mechanical performance of polymeric parts produced by multi jet fusion and selective laser sintering. *Journal of Manufacturing Processes*, *65*, 271-282.

Cano, A. J., Salazar, A., & Rodríguez, J. (2018). Effect of temperature on the fracture behavior of polyamide 12 and glass-filled polyamide 12 processed by selective laser sintering. *Engineering Fracture Mechanics*, *203*, 66-80.

Caulfield, B., McHugh, P. E., & Lohfeld, S. (2007). Dependence of mechanical properties of polyamide components on build parameters in the SLS process. *Journal of Materials Processing Technology*, *182*(1-3), 477-488.

Charoo, N. A., Barakh Ali, S. F., Mohamed, E. M., Kuttolamadom, M. A., Ozkan, T., Khan, M. A., & Rahman, Z. (2020). Selective laser sintering 3D printing–an overview of the technology and pharmaceutical applications. *Drug Development and Industrial Pharmacy*, *46*(6), 869-877.

Dadbakhsh, S., Verbelen, L., Verkinderen, O., Strobbe, D., Van Puyvelde, P., & Kruth, J.-P. (2017). Effect of PA12 powder reuse on coalescence behaviour and microstructure of SLS parts. *European Polymer Journal*, *92*, 250-262.

de Oliveira Setti, G., Fernandes de Oliveira, M., Alves Maia, I., Vicente Lopes da Silva, J., Savu, R., & Joanni, E. (2014). Correlation between mechanical and surface properties of SLS parts. *Rapid Prototyping Journal*, *20*(4), 285-290.

Dupin, S., Lame, O., Barrès, C., & Charmeau, J.-Y. (2012). Microstructural origin of physical and mechanical properties of polyamide 12 processed by laser sintering. *European Polymer Journal*, *48*(9), 1611-1621.

El Magri, A., Bencaid, S. E., Vanaei, H. R., & Vaudreuil, S. (2022). Effects of Laser Power and Hatch Orientation on Final Properties of PA12 Parts Produced by Selective Laser Sintering. *Polymers*, *14*(17), 3674.

Hopkinson, N., Majewski, C. E., & Zarringhalam, H. (2009). Quantifying the degree of particle melt in Selective Laser Sintering®. *CIRP Annals*, *58*(1), 197-200.

Majewski, C., Zarringhalam, H., & Hopkinson, N. (2008). Effect of the degree of particle melt on mechanical properties in selective laser-sintered Nylon-12 parts. *Proceedings of the Institution of Mechanical Engineers, Part B: Journal of Engineering Manufacture*, *222*(9), 1055-1064.

Mwania, F. M., Maringa, M., & Van der Walt, K. (2020). A review of methods used to reduce the effects of high temperature associated with polyamide 12 and polypropylene laser sintering. *Advances in Polymer Technology*, *2020*, 1-11.

Obst, P., Launhardt, M., Drummer, D., Osswald, P. V., & Osswald, T. A. (2018). Failure criterion for PA12 SLS additive manufactured parts. *Additive Manufacturing*, *21*, 619-627.

Olejarczyk, M., Gruber, P., & Ziółkowski, G. (2020). Capabilities and limitations of using Desktop 3-D printers in the laser sintering process. *Applied Sciences*, *10*(18), 6184.

Rajesh, R., Sudheer, S., & Kulkarni, M. V. (2015). Selective laser sintering process–a review. *Int. J. Curr. Eng. Sci. Res*, *2*, 2393-8374.

Rodríguez, A. G., Mora, E. E., Velasco, M. A., & Tovar, C. A. N. (2023). Mechanical properties of polyamide 12 manufactured by means of SLS: Influence of wall thickness and build direction. *Materials Research Express*, *10*(10), 105304.

Rosso, S., Meneghello, R., Biasetto, L., Grigolato, L., Concheri, G., & Savio, G. (2020). In-depth comparison of polyamide 12 parts manufactured by multi jet fusion and selective laser sintering. *Additive Manufacturing*, *36*, 101713.

Roszak, R., Schob, D., Sagradov, I., Kotecki, K., Sparr, H., Maasch, P., Franke, R., & Ziegenhorn, M. (2021). Experimental determination and numerical simulation of temperature dependent material and damage behaviour of additively manufactured polyamide 12. *Mechanics of Materials*, *159*, 103893.

Schob, D., Richter, L., Kotecki, K., Kurpisz, D., Roszak, R., Maasch, P., & Ziegenhorn, M. (2023). Characterization and simulation of shear-induced damage in selective-laser-sintered polyamide 12. *Materials*, *17*(1), 38.

Schob, D., Roszak, R., Sagradov, I., Sparr, H., Ziegenhorn, M., Kupsch, A., Léonard, F., Müller, B., & Bruno, G. (2019). Experimental determination and numerical simulation of material and damage behaviour of 3D printed polyamide 12 under quasi-static loading. *Archives of Mechanics, 71*(4-5), 507-526.

Senthilkumaran, K., Pandey, P. M., & Rao, P. V. M. (2009). Influence of building strategies on the accuracy of parts in selective laser sintering. *Materials & Design*, *30*(8), 2946-2954.

Simha Martynková, G., Slíva, A., Kratošová, G., Čech Barabaszová, K., Študentová, S., Klusák, J., Brožová, S., Dokoupil, T., & Holešová, S. (2021). Polyamide 12 materials study of morpho-structural changes during laser sintering of 3d printing. *Polymers*, *13*(5), 810.

Sindinger, S.-L., Kralovec, C., Tasch, D., & Schagerl, M. (2020). Thickness dependent anisotropy of mechanical properties and inhomogeneous porosity characteristics in laser-sintered polyamide 12 specimens. *Additive Manufacturing*, *33*, 101141.

Stichel, T., Frick, T., Laumer, T., Tenner, F., Hausotte, T., Merklein, M., & Schmidt, M. (2017). A Round Robin study for selective laser sintering of polyamide 12 : Microstructural origin of the mechanical properties. *Optics & Laser Technology*, *89*, 31-40.

Stoia, D. I., Linul, E., & Marsavina, L. (2019). Influence of manufacturing parameters on mechanical properties of porous materials by selective laser sintering. *Materials*, *12*(6), 871.

Tomanik, M., Żmudzińska, M., & Wojtków, M. (2021). Mechanical and structural evaluation of the PA12 desktop selective laser sintering printed parts regarding printing strategy. *3D Printing and Additive Manufacturing*, *8*(4), 271-279.

Toth-Taşcău, M., Raduta, A., Stoia, D. I., & Locovei, C. (2012). Influence of the Energy Density on the Porosity of Polyamide Parts in SLS Process. *Solid State Phenomena*, *188*, 400-405.

Usher, J. S., Gornet, T. J., & Starr, T. L. (2013). Weibull growth modeling of laser-sintered nylon 12. *Rapid Prototyping Journal*, *19*(4), 300-306.

Zárybnická, L., Petrů, J., Krpec, P., & Pagáč, M. (2022). Effect of Additives and Print Orientation on the Properties of Laser Sintering-Printed Polyamide 12 Components. *Polymers*, *14*(6), 1172.

Author(s) Information

Boukhoulda Farouk Benallel
Djillali Liabes University of Sidi Bel Abbes, Department of Mechanics, Faculty of Technology, Laboratory of Structural and Solid Mechanics, P.O. Box 89, Ben Mhidi City, Sidi Bel Abbes, 22000, Algeria
Contact e-mail: *farouk.boukhoulda@univ-sba.dz*

Djellal Kouider
Djillali Liabes University of Sidi Bel Abbes, Department of Mechanics, Faculty of Technology, Laboratory of Structural and Solid Mechanics, P.O. Box 89, Ben Mhidi City, Sidi Bel Abbes, 22000, Algeria

Bendine Kouider
Djillali Liabes University of Sidi Bel Abbes, Department of Mechanics, Faculty of Technology, Laboratory of Structural and Solid Mechanics, P.O. Box 89, Ben Mhidi City, Sidi Bel Abbes, 22000, Algeria

Boukhoulda Abdelaziz
Djillali Liabes University of Sidi Bel Abbes, Department of Mechanics, Faculty of Technology, Laboratory of Structural and Solid Mechanics, P.O. Box 89, Ben Mhidi City, Sidi Bel Abbes, 22000, Algeria

To cite this article:

Benallel, B. F., Kouider, D., Kouider, B., & Abdelaziz, B. (2025). Impact of printing orientation on the mechanical properties of selectively laser sintered PA12. *The Eurasia Proceedings of Science, Technology, Engineering and Mathematics (EPSTEM), 38,* 401-414.